# Approximating stable and unstable manifolds in experiments

Ioana Triandaf,[1] Erik M. Bollt,[2] and Ira B. Schwartz[1]
[1]*Code 6792, Plasma Physics Division, Naval Research Laboratory, Washington, DC 20375*
[2]*Department of Mathematics and Computer Science, Clarkson University, P.O. Box 5815, Potsdam, New York 13699*
(Received 5 August 2002; revised manuscript received 23 December 2002; published 12 March 2003)

We introduce a procedure to reveal invariant stable and unstable manifolds, given only experimental data. We assume a model is not available and show how coordinate delay embedding coupled with invariant phase space regions can be used to construct stable and unstable manifolds of an embedded saddle. We show that the method is able to capture the fine structure of the manifold, is independent of dimension, and is efficient relative to previous techniques.

DOI: 10.1103/PhysRevE.67.037201 PACS number(s): 05.45.Ac, 42.60.Mi

Many nonlinear phenomena can be explained by understanding the behavior of the unstable dynamical objects present in the dynamics. Dynamical mechanisms underlying chaos may be described by examining the stable and unstable invariant manifolds corresponding to unstable objects, such as saddles [1]. Applications of the manifold topology have contrubuted towards understanding of chaos [2], chaotic saddle dynamics [3], boundary crises [4], and have been used in real applications, such as algorithms for sustaining chaos [5,6], communicating with chaos [7], and preventing resonances in mechanics by spreading modal energy in continua [8], to name just a few. Despite the central importance of stable and unstable manifolds of unstable saddle orbits, these structures have been previously entirely inaccessible to experimental data, in the absence of a closed form model. There has been a great deal of effort put forth to compute these structures theoretically when a model is known, based on the stable manifold theorem. For manifolds of one dimension, model based methods have been used such as those in Refs. [9,10] while techniques for two-dimensional dimensional methods have appeared in Refs. [11–13]. Techniques known as the ''sprinkler method,'' which also assume that a model is known *a priori*, have appeared in Refs. [14–16]. In this paper, we put forth a method intended to remedy the gap between theory and experiment by obtaining a qualitative reconstruction of the stable and unstable manifolds when only experimental data are available. Moreover, we illustrate how errors propagate in the technique by considering the complexity of the method. This has not been done previously in Refs. [14–16].

We introduce a computational procedure to construct the stable and unstable manifolds of a saddle directly from data. A random mesh of initial conditions is used to generate trajectories that remain near the saddle for long sojourns. We show that these initial conditions, along with their first few iterations, allow embedding techniques to be applied [17,18]. We apply the algorithm to a model of the $CO_2$ laser:

$$Z'(t) = -[\Delta \cos(\Omega t) - S], \tag{1}$$

$$S'(t) = -\epsilon_1 s - e^Z - \epsilon_2 S e^Z + 1,$$

where $I = e^Z$ and $S$ denote (scaled) intensity and population inversion [19]. Fixed parameters are $\epsilon_1 = 0.09$, $\epsilon_2 = 0.003$, $\Omega = 0.9$, and $\Delta = 1.88$.

We consider a basin saddle of Eq. (1) which lies on the basin boundary between a chaotic attractor and a period-four periodic attractor. The chosen parameters are in a region in which the chaotic attractor disappears and only a periodic attractor persists along with chaotic transients due to intersecting stable and unstable manifolds of the basin saddle. Figure 1 depicts stable and unstable manifolds of the basin saddle calculated by traditional techniques [10]. We have chosen this parameter set precisely for its difficulty in computing the invariant manifolds of unstable saddles.

We describe our procedure using the model in Eq. (1) and reconstruct the stable and unstable manifolds of the unstable saddle [20], produced traditionally in Fig. 1 in the variables $(S,I)$. Pick a region of interest to be a box $B$ of Fig. 1 containing the unstable saddle with part of its stable and unstable manifolds. Inside that box we randomly pick a large number $N$ of initial conditions $(S_{0_i}, I_{0_i})_{i=1,N}$ and record which of these initial conditions will generate trajectories

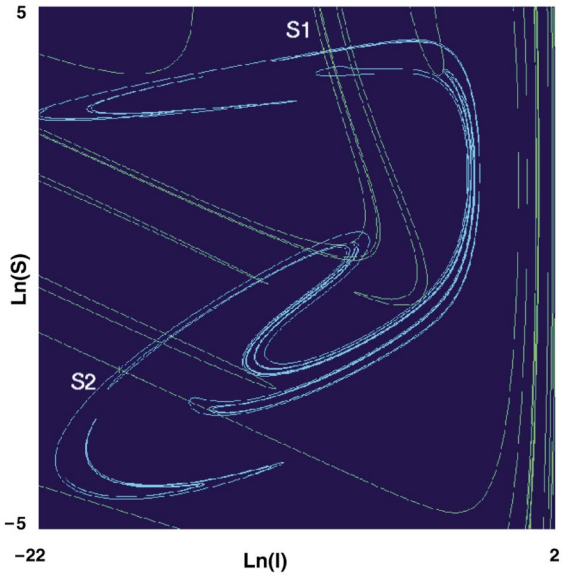


FIG. 1. (Color) The stable and unstable manifolds of the laser model in Eq. (1) directly computed by traditional numerical analytic techniques of Ref. [10]. $S_1$ and $S_2$ denote the period-two basin boundary saddle. The unstable manifold is shown in bright white in the center of the figure and includes a chaotic saddle.

 

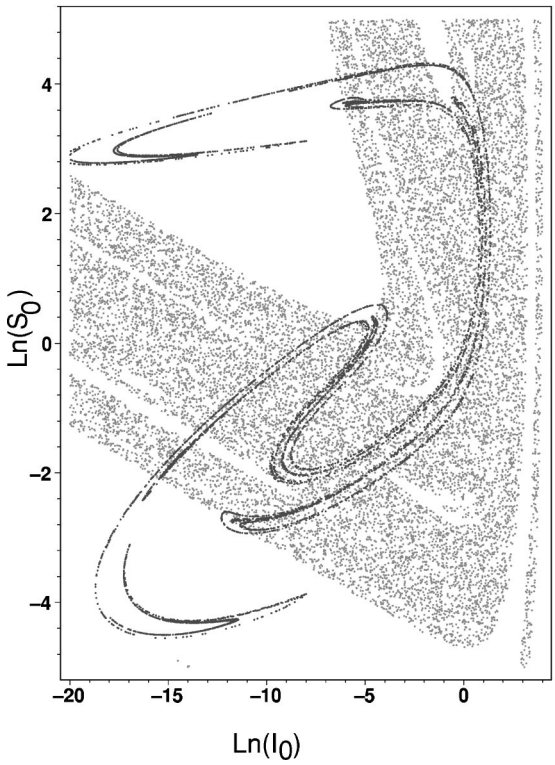


FIG. 2. Initial conditions $\{(S_{0_i},I_{0_i})\}_{i=1}^{N}$ of Eq. (1) whose trajectories remain in the box for a lifetime of at least $n=200$ iterations, and their last observed end points, $\{(S_{n_i},I_{n_i})\}_{i=1}^{N}$. Observe that the area covered by the points $\{(S_{0_i},I_{0_i})\}_{i=1}^{N}$ closely approximates the stable manifold in Fig. 1, and the points $\{(S_{n_i},I_{n_i})\}_{i=1}^{N}$ approximate the unstable manifolds.

remaining in the box for a large number of iterations. For the laser model above, a good threshold was to retain the initial conditions that generate trajectories remaining in the box for no less then $n=200$ periods of the drive. In addition, we monitor a small neighborhood of the period-four attracting orbit *A*, which also is contained in *B*, and eliminate any points converging to this attractor since these points will not represent the manifolds we approximate.

Computational approximations to stable and unstable manifolds are shown in Fig. 2. We algorithmically summarize our procedure used to generate Fig. 2.

(0) Fix a box $B=[a,b]\times[c,d]$ of interest, in the space $(S,I)$, and $A\subset B$.

(1) Pick a random initial condition $(S_0,I_0)$ and run the system for *n* iterations. In this case, we chose $n=200$.

(2) If the entire *n*-step trajectory in part 1 lies within *B*, and does not converge to set *A*, then record the corresponding initial conditions $(S_0,I_0)$ to a file *and* record the end point that was the last observed point within the box, $(S_n,I_n)$.

(3) Repeat steps 1 and 2 for *N* randomly chosen initial conditions.

(4) Plot the initial conditions $\{(S_{0_i},I_{0_i})\}_{i=1}^{N}$ saved in step 3, thus producing the stable manifolds in Fig. 2, and plot the end points $\{(S_{n_i},I_{n_i})\}_{i=1}^{N}$ that produce the unstable manifolds in Fig. 2.

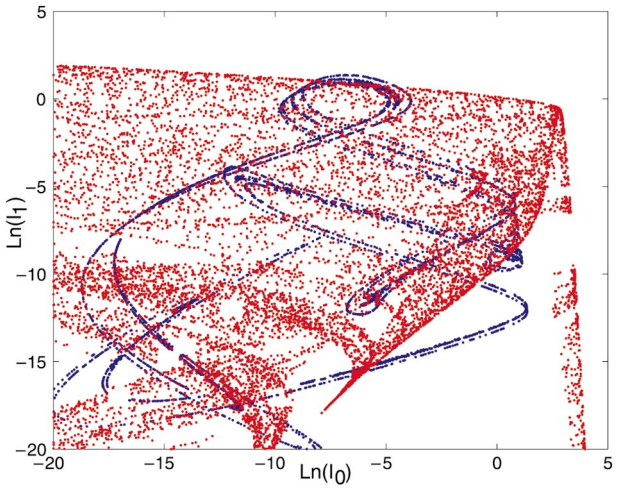


FIG. 3. (Color) Intensity delay variables $(I_0,I_1)$ that generate trajectories that remain in the box shown for $n=200$ iterations reveal structures that resemble the stable (red) manifolds in Figs. 1 and 2, and likewise the ending points $(I_n,I_{n+1})$ apparently reveal the unstable (blue) manifolds.

An essential feature of this algorithm is that the computational complexity to produce Fig. 2 is quite different as compared to the traditional production used for Fig. 1. Our algorithm is: (1) simpler, (2) faster, and (3) experimentally accessible. We will investigate properties (1) and (2) at the end of the paper, but first we discuss (3).

In a real driven laser experiment one cannot measure the population inversion. Instead, we can reconstruct the dynamical objects by delay embedding of the only directly observable quantity: intensity measurements. The procedure needs to be adapted only slightly. To generate additional variables we use the value of the intensity after one period $I_1$. The reconstructed stable manifold in $(I_0,I_1)$ space is shown in Fig. 3. In general, the Takens embedding theorem [21] tells us that to unfold an object embedded on a *d*-dimensional manifold may require up to $2d+1$ delay variables. The Sauer-Yorke embedology theorem [22] has sharpened this estimate to allow for *d* to be the fractal dimension. Since Eq. (1) evolves in the plane, $d=2$ suggests that up to five delay variables may be necessary to unfold all possible intersections. Comparing Figs. 2 and 3 we notice the fine fractal structure. Still, in Fig. 3, there are self-intersections that cannot be found in Fig. 2. In Fig. 4, we show the reconstructed manifold in three dimensions, using the three variables of intensity at three delayed times $(I_0,I_1,I_2)$. Viewed from many angles (only one view can be shown here) reveals no apparent self-intersections and the character of the invariant set in Fig. 3 is apparently the same as the invariant set in Fig. 2.

To initiate the above algorithm with intensity alone, in three delays, we restate the period-two saddle as $I_1=(I_{0_1},I_{1_1},I_{2_1})$ and $I_2=(I_{0_2},I_{1_2},I_{2_2})$. It will be necessary to choose a bounding box $[a,b]\times[a,b]\times[a,b]$ that contains $I_1;I_2$, but if *all* of the experimental data are kept during the experiment run time, then the thresholds *a* and *b* can be chosen to produce a relevant basin plot. Otherwise, the above

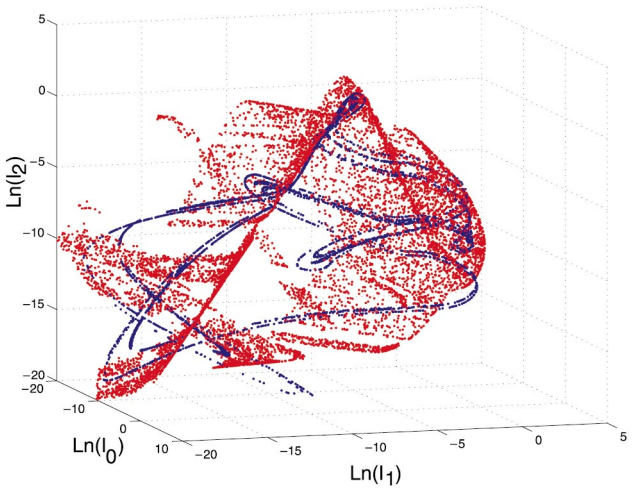


FIG. 4. (Color) Intensity delay variables $(I_0, I_1, I_2)$ that generate trajectories that remain in the box shown for $n=200$ iterations reveal structures that resemble the stable (red) manifolds in Figs. 1 and 2, and likewise the ending points $(I_n, I_{n+1}, I_{n+2})$ apparently reveal the unstable (blue) manifolds.

algorithm is essentially the same, except we record and plot initial thresholds, and their two-step delays, which stay in the box. See Figs. 3 and 4 for results. We remark here that in the presence of noise perturbations up to 4% in the intensity sequence, the same structure is present in Fig. 4.

We now compare the computational complexity of our calculation with that of the more traditional technique [10] based on the the stable manifold theorem. For concreteness and ease of calculation, we analyze both techniques assuming application to searching for unstable manifolds in a Smale horseshoe [23]. Stable manifolds are considered similarly.

First we discuss the traditional technique, in a simplified form. The stable manifold theorem [24] provides the simplest algorithm to numerically follow unstable manifolds: place an $\epsilon$-spaced grid along $E^u$, a small eigenvector of the unstable saddle point, of length $\delta$; thus $M_0=\delta/\epsilon$ points are used. Upon iteration, these points stretch apart at a rate $\lambda_u > 1$, the unstable Lyapunov number, but are compressed toward the full nonlinear manifold $W^u$ at a rate $\lambda_s<1$ factor upon each iteration. Therefore, to maintain an $\epsilon$-plot resolution, it is necessary to insert extra grid points upon each iteration, so that the distance between any two grows by more than $\epsilon$. At the $n$th iteration, the number of added points is $M_n=\lambda_u^n\delta/\epsilon$, and the total number of grid points that must be tracked during $n$ iterates of the initial vector follows

$$M=\frac{\delta}{\epsilon}\sum_{i=0}^{n}\lambda_u^i=\frac{\delta}{\epsilon}\left(\frac{\lambda_u^{1+n}-1}{\lambda_u-1}\right). \tag{2}$$

The total manifold length yielded is

$$L_{\text{total}}=\delta\left(\frac{\lambda_u^{1+n}-1}{\lambda_u-1}\right), \tag{3}$$

but most of this length is not within an $s\times s$ box window $V$ of interest. For large $n$, there are long segments of unstable manifold that stretch far outside the window of interest. Since the standard Smale horseshoe is used, we let $f=2$ be the number of "folds" introduced at each $m$ step. Let $m=n-q$ be the time after which the initial $\delta$ vector stretches across the box, in $q$ iterations, where $q$ solves, $\delta(\lambda_u^{1+q}-1/\lambda_u-1)=s$. Thus, the total length of unstable manifold in the window follows

$$L_{\text{in}}=s\sum_{i=0}^{m}sf^i=s\left(\frac{f^{1+m}-1}{f-1}\right). \tag{4}$$

We define an efficiency factor,

$$\mathcal{E}_n=\frac{(\text{No. of grid pts. in window})}{(\text{No. of total gridpts.})}=\frac{L_{\text{in}}}{\epsilon M}$$

$$=\frac{s(f^{1+m}-1)(\lambda_u-1)}{\delta(f-1)(\lambda_u^{n+1}-1)}, \tag{5}$$

where $0\leqslant\mathcal{E}\leqslant 1$, and bigger is more efficient.

Efficiency of our technique applied to the same horseshoe follows a very different and essentially probabilistic calculation. Since the $n$-step forward invariant set of the Smale horseshoe is essentially $f^n$ horizontal strips, for an $f$-times folding horseshoe, then the area of the $n$-step invariant set is $I_n=(f\lambda_s)^n s^2$. We assume that points that leave $V$ never return. The fraction of invariant points in $V$ follows

$$\mathcal{E}_n=\frac{m(I_n)}{m(B)}=(f\lambda_s)^n, \tag{6}$$

where $m(\cdot)$ denotes Lebesgue measure. Therefore, the expected number of invariant points $\langle M_{\text{in}}\rangle$, due to uniformly sampling $M$ initial conditions in $B$, is

$$\langle M_{\text{in}}\rangle=M\mathcal{E}_n. \tag{7}$$

We again ask how big must $M$ be for an expected $\epsilon$ plot. Given $f^n$ strips, each of size $\lambda_s^n\times s$, $\langle q\rangle$, the expected number of points in each strip, is

$$\langle q\rangle=\frac{\langle M_{\text{in}}\rangle}{f^n}=M\lambda_s^n. \tag{8}$$

Therefore, the expected spacing between points in any given strip is

$$\langle\epsilon\rangle=\frac{s}{\langle q\rangle}, \tag{9}$$

from which follows

$$\langle M\rangle=\frac{s}{\langle\epsilon\rangle\lambda_s^n}. \tag{10}$$

The most striking feature of the efficiencies of the two techniques, as reflected by contrasting Eq. (5) versus Eq. (6),

and also Eq. (2) versus Eq. (10), is that the complexity of the stable-manifold based technique compounds with the unstable Lyapunov number, while it is the stable Lyapunov number that moderates the complexity of our new probabilistic algorithm. Therefore, the relative sizes of $\lambda_u$ and $\lambda_s$ ultimately determine which approach is more efficient. We emphasize that $n$ for the traditional technique is moderated by Eq. (4), and is essentially fixed by the amount of manifold length wished in the screen as one grows the unstable manifold. That is quite different from the $n$ for our probabilistic algorithm, which is chosen *a priori* as the lifetime in the box $W$ of an initial condition. As we have developed, $f$ moderates the number of folds of the unstable manifold which can be resolved.

In conclusion, the procedure described to approximate invariant unstable and stable manifolds via experimental procedures is computationally efficient, and independent of phase space dimension. We have shown that these invariant structures are accessible to an experimentalist, using only time-delay embeddings of a measured data set, which has been suitably restricted as we have described. Compared to other methods [10,25] the length of the segment of manifold which is identified is not as seriously restricted in this algorithm. (The Lyapunov numbers of the governing saddle are $\lambda_u = 3.9$, $\lambda_s = 0.06$. For the example considered here, our method is estimated to be more than 1000 times faster than the segments methods such as in Ref. [10]. Error analysis also shows that with $n = 50$ iterates, no discernible changes in the results are observed.) The current procedure was applied to reveal the stable manifolds of a basin saddle that is known [4] to form the basin boundary between attractors. So, in particular, the above procedure can be used not only to increase the predictability of experimental dynamics, but can also be especially helpful in control algorithms for sustaining chaos such as in Ref. [6].

I.B.S. and I.T. are supported by the Office of Naval Research. E.B. is supported by the National Science Foundation under Grant No. DMS-0071314.

[1] V.K. Melnikov, Trans. Moscow Math. Soc. **12**, 1 (1963).
[2] J. Guckenheimer and P. Holmes, *Nonlinear Oscillations, Dynamical Systems, and Bifurcations of Vector Fields* (Springer-Verlag, New York, 1983).
[3] H.E. Nusse and J.A. Yorke, Physica D **36**, 187 (1989).
[4] C. Grebogi, E. Ott, and J.A. Yorke, Physica D **7**, 181 (1983).
[5] I. Schwartz and I. Triandaf, Phys. Rev. Lett. **77**, 4740 (1996).
[6] I. Triandaf and I.B. Schwartz, Phys. Rev. E **62**, 3529 (2000).
[7] G.D. VanWiggeren and R. Roy, Science **279**, 1198 (1998).
[8] I.B. Schwartz and I.T. Georgiou, Phys. Lett. A **242**, 307 (1998).
[9] T. Valkering, J. Phys. A **17**, 3135 (1984).
[10] Z. You, E.J. Kostelich, and J.A. Yorke, Int. J. Bifurcation Chaos Appl. Sci. Eng. **1**, 605 (1991).
[11] B. Krauskopf and H. Osinga, J. Comput. Phys. **146**, 404 (1998).
[12] B. Krauskopf and H. Osinga, Chaos **9**, 768 (1999).
[13] N. Smaoui, SIAM (Soc. Ind. Appl. Math.) J. Sci. Stat. Comput. **23**, 824 (2001).
[14] G. Hus, E. Ott, and C. Grebogi, Phys. Lett. A **127**, 199 (1988).
[15] Y.-C. Lai, T. Tel, and C. Grebogi, Phys. Rev. E **48**, 709 (1993).
[16] J. Aquirre, J.C. Vallejo, and M.A.F. Sanjuan, Phys. Rev. E **64**, 066208 (2003).
[17] T. Sauer, J.A. Yorke, and M. Casdagli, J. Stat. Phys. **65**, 579 (1991).
[18] D.S. Broomhead and G.P. King, Physica D **20**, 21 726 (1986).
[19] I.B. Schwartz, Phys. Rev. Lett. **60**, 1359 (1988).
[20] D.P. Lathrop and E.J. Kostelich, Phys. Rev. A **40**, 4028 (1989).
[21] F. Takens, Lect. Notes Math. **898**, 366 (1980).
[22] T. Sauer, J. Yorke, and M. Casdagli, J. Stat. Phys. **65**, 579 (1991).
[23] S. Smale, Bull. Am. Math. Soc. **73**, 747 (1967).
[24] C. Robinson, *Dynamical Systems: Stability, Symbol Dynamics, and Chaos* (CRC Press, Ann Arbor, 1995).
[25] W. Franceschini and L. Russo, J. Stat. Phys. **25**, 757 (1981).